Electronic Supplementary Material (ESI) for ChemComm.

Nanoplasmonic Ruler to Measure Lipid Vesicle Deformation

Supporting Information

Joshua A. Jackman,[a] Barbora Špačková,[c] Eric Linardy, [a] Min Chul Kim,[a] Bo Kyeong Yoon,[a] Jiří Homola[c] and Nam-Joon Cho[a,b]

[a]School of Materials Science and Engineering and Centre for Biomimetic Sensor Science, Nanyang Technological University, 50 Nanyang Avenue 639798, Singapore. E-mail: njcho@ntu.edu.sg; Tel: +65-6592-7945
[b]School of Chemical and Biomedical Engineering, Nanyang Technological University, 62 Nanyang Drive 637459, Singapore.
[c]Institute of Photonics and Electronics, Academy of Science of the Czech Republic, Chaberska 57, Prague 8 18251, Czech Republic.

Experimental Section

Vesicle Preparation. The extrusion method was utilized to prepare lipid vesicles of controlled size distribution. The lipid composition was 100 mol% 1-palmitoyl-2-oleyl-*sn*-glycero-3-phosphocholine (POPC) (Avanti Polar Lipids, Alabaster, AL) for most experiments. In some exceptions where noted, the lipid composition was 50/50 mol% POPC and positively charged 1-palmitoyl-2-oleoyl-*sn*-glycero-3-ethylphosphocholine (POEPC) lipid. For fluorescence microscopy experiments, 0.5 wt% Lissamine Rhodamine B 1,2-Dihexadecanoyl-sn-Glycero-3-Phosphoethanolamine, Triethylammonium Salt (rhodamine DHPE) (Life Technologies, Carlsbad, CA) was also included in the lipid mixture. Initially, as-supplied lipids were dispersed in chloroform and then the chloroform was evaporated by drying with nitrogen gas, which yielded a dried lipid film. The film was stored inside a vacuum desiccator for at least 12 hours. Then, aqueous buffer solution (10 mM Tris [pH 7.5] with 150 mM NaCl) was added to the dried lipid film, and the lipids were resuspended by vortexing at high speed at a nominal lipid concentration of 5 mg/mL. Unless otherwise noted, lipid vesicles were next extruded using a MiniExtruder apparatus (Avanti Polar Lipids) and passed through track-etched polycarbonate membranes of decreasing pore diameter (30, 50, or 100 nm) for a minimum of 17 cycles per membrane in order to form small unilamellar vesicles (~70 nm diameter). After preparation, the vesicle suspensions were stored at 4 °C and used for experiment within 48 hours, with appropriate dilution immediately preceding experiment. All buffer solutions were prepared using deionized water (18.2 MΩ·cm resistivity) that had been treated by the Milli-Q filtration system (Millipore, Billerica, MA).

Dynamic Light Scattering. The size distribution of the extruded vesicles, in terms of the hydrodynamic diameter of extruded vesicles undergoing Brownian motion in suspension, was measured by a 90Plus particle size analyzer (Brookhaven Instruments, Holtsville, NY). A

monochromatic 658.0 nm laser light was transmitted through the vesicle suspension and light was scattered by vesicles in solution. All measurements were performed at a scattering angle of 90° at 25 °C. The temporal shifts in the intensity of the scattered light are related to the diffusion coefficient of the vesicles, and according to the Stokes-Einstein equation, the diffusion coefficient is inversely proportional to the hydrodynamic diameter of the vesicles. The temporal fluctuation in the intensity of the scattered light was measured and the signal was expressed in terms of an autocorrelation function. The autocorrelation function of the intensity signal was recorded and analyzed by the cumulants method. The analysis yielded the intensity-weighted vesicle size distribution, including average effective hydrodynamic diameter and sample polydispersity.

Localized Surface Plasmon Resonance (LSPR) Spectroscopy. Indirect nanoplasmonic sensing (INPS) measurements of vesicle adsorption and rupture were conducted using an XNano instrument (Insplorion AB, Gothenburg, Sweden). Ensemble-averaged recordings in optical transmission mode were recorded on glass sensor chips (Insplorion AB) with deposited gold nanodisks, as fabricated by hole-mask colloidal lithography. The gold nanodisks had a surface coverage of ~8% and were coated with an approximately 10-nm thick layer of sputter-deposited titanium oxide or silicon oxide. The experimental procedure, substrate cleaning, and data analysis were performed, as previously described[1]. Liquid sample was introduced into the measurement chamber at a continuous flow rate of 100 µL/min (average flow velocity: 50 mm/min). The bulk refractive index sensitivity of the chips was determined by titration with a series of glycerol/water mixtures with known refractive indices as determined using an Abbe refractometer (NAR-1T Liquid, ATAGO Co., Tokyo, Japan).

Fluorescence Recovery After Photobleaching (FRAP) Analysis. Epifluorescence microscopy on supported lipid bilayers was conducted using an inverted optical microscope (Eclipse TI-U

microscope; Nikon, Japan) that has a 60× magnification (NA=1.49) oil immersion objective (Nikon) and TRITC (rhodamine-DHPE) filter set. Images were captured using an iXon EMCCD camera (Andor Technology, Northern Ireland), with a mercury lamp illumination source (Intensilight C-HGFIE, Nikon). The recorded images consisted of 512 × 512 pixels with a pixel size of 0.267 × 0.267 μm. FRAP analysis was performed by photobleaching with a 532 nm, 100 mW laser beam. After bleaching, recovery of fluorescence intensity in the 30 μm wide circular, bleached spot was monitored as a function of time and recovery profile was analyzed by the Hankel transform method. Experiments were performed on glass coverslips (Menzel Gläser, Braunschweig, Germany), or silicon oxide-coated XNano sensor chips. Both types of substrates were attached to a microfluidic flow cell (stick-Slide I0.1 Luer, Ibidi, Munich, Germany), which was connected to a peristaltic pump for liquid exchange in the measurement chamber. An injection flow rate of 50 μL/min was used in all experiments.

Scanning Electron Microscopy. The samples were coated with a thin layer of platinum with a JFC-1600 sputter coater (Auto Fine Coater, JEOL, Tokyo, Japan) (20 mA, 60 sec). SEM imaging was performed using a FESEM 7600F instrument (JEOL, Japan) with an acceleration voltage of 5 kV at different magnifications.

Finite-Difference Time-Domain Simulations. The simulations were carried out using the 3D finite-difference time-domain method (FDTD, Lumerical). The extinction of the substrate q_{ext} was calculated as $q_{ext} = \sigma c_{ext}^{0}$ where σ stands for the surface density of nanodisks and c_{ext}^{0} stands for the extinction cross-section of a single nanodisk which was determined using the total-field scattered-field source. A tapered gold nanodisk with bottom diameter 95 nm, top diameter 85nm and height 30nm on the glass substrate was assumed, with surface density σ = 10 $NP/\mu m^2$ for surface sensitivity analysis and the structure was covered with 10-nm thick sputtered layer of

titanium oxide or silicon oxide coating. Refractive indices of the titanium oxide and silicon oxide sputtered coatings were taken from ellipsometry measurements which were performed using identically prepared glass substrates without nanodisks. The refractive indices at 700 nm were 2.32 and 1.97 for the titanium oxide- and silicon oxide-coated substrates, respectively. The dielectric constant of gold was taken from Ref. 2, and the refractive indices of the glass substrate and water were 1.45 and 1.33, respectively. A grid size of 0.75 nm was chosen for the simulations.

Theoretical Aspects

The core aspects of this model are originally presented in Ref. 3, 4 and extended here in order to explain the basic principles behind the measurement of vesicle deformation. The electromagnetic field is highly concentrated at the edges of the gold nanodisk and decreases proportionally to $1/(z+R_*)^3$ where z is the coordinate perpendicular to the substrate surface ($z=0$ corresponds to the vesicle-substrate contact) and R_* is the length scale characterizing the distance between the center of the nanodisk and vesicle-substrate contact. The corresponding contribution to the LSPR peak shift due to the refractive index change, $\Delta\lambda_{max}$, is then proportional to $1/r^6$ and can be represented as

$$\Delta\lambda_{max} = S_B \int_0^\infty \frac{5R_*^5}{(R_*+z)^6}\Delta n(z)dz, \quad (1)$$

where S_B is sensitivity to the refractive index change in the whole medium (bulk sensitivity) and $\Delta n(z)dz$ is the spatial distribution of the refractive index change. According to Eq. (1), the sensitivity to a refractive index change occurring within a layer with a thickness D (surface sensitivity) can be defined as

$$S_S = \frac{\Delta\lambda_{max}}{\Delta n} = S_B\left[1-\left(\frac{R_*}{D+R_*}\right)^5\right]. \quad (2)$$

In the case of vesicles attached to the surface, $\Delta n(z)dz$ can be rewritten as $Cln_L dA$ where C is the surface concentration of vesicles, l and n_L are the thickness and refractive index of the lipid bilayer, respectively, and dA is the area segment of a vesicle. In the case of spherically shaped vesicles, $dA = 2\pi r dz$, where r is the vesicle radius in solution in the non-deformed state and Eq. (1) can be written as

$$\Delta\lambda_{max} = 2\pi r Cln_L S_B \int_0^{2r} \frac{5R_*^5}{(R_*+z)^6} dz \quad (3)$$

We recall general equations that were presented in Ref. 4 in order to show the effect of deformation of adsorbed vesicles on the LSPR signal. An adsorbed vesicle is represented as a truncated sphere with a circular vesicle-substrate contact area of radius a. During deformation, the total vesicle area is conserved. For this reason, its radius, r_*, is slightly larger than that in solution. The vesicle shape characteristics are characterized by a dimensionless parameter defined as $p \equiv a/r$. In particular, the ratio of the radii for adsorbed vesicles in the deformed and non-deformed cases is determined as

$$\frac{r_*}{r} = \frac{4-p^2}{(16-8p^2)^{1/2}}, \quad (4)$$

where $r_* > r$ while the difference in vesicle height is expressed via r_* and a as

$$h = r_* + (r_*^2 - a^2)^{1/2}. \quad (5)$$

With this specification, the area segment of deformed vesicle is $2\pi r_* dz$ for the out of contact area and πa^2 for the contact area. In particular, Eq. (3) can be generalized as

$$\Delta\lambda_{\max} = \pi Cln_L S_B \left(\frac{5a^2}{R_*} + 2r_* \int_0^h \frac{5R_*^5}{(R_*+z)^6} dz\right). \quad (6)$$

As shown earlier,[3] the scale of the interval making the main contribution to the integrals in Eqs. (3) and (6) is $\Delta z \cong R_*/5$. This interval is usually appreciably smaller than the vesicle size.

For this reason, the integrations in Eqs. (3) and (6) can be extended to infinity, and one can rewrite Eqs. (3) and (6), respectively, as

$$\Delta\lambda_{\max} = 2\pi r C l n_L S_B, \tag{7}$$

$$\Delta\lambda_{\max} = \pi C l n_L S_B \left(\frac{5a^2}{R_*} + 2r_*\right), \tag{8}$$

In analogy to Ref. 4, we define

$$P \equiv \frac{5a^2}{2rR_*} + \frac{r_*}{r}, \tag{9}$$

to be a measure of the effect of deformation of single vesicles on the LSPR signal. By definition, the effect is calculated with respect to less deformed or non-deformed vesicles. Due to deformation, vesicles become closer to the gold nanoparticles, and their contributions to $\Delta\lambda_{\max}$ increases, and accordingly $P \geq 1$. The ratio P [Eq. (9)] is computed as a function of a/r changing in the range from 0 to 1 (the latter corresponds to appreciably deformed vesicles). With increasing a/r, P rapidly increases. The values of a/r were calculated for r = 35 nm (determined by dynamic light scattering measurements) and R_*= 74 nm (determined by FDTD simulation results). Using Eqs. (8) and (9) and assuming the thickness and refractive index of the lipid bilayer does not change, the deformation of the vesicles on different substrates can be compared using

$$\frac{P_1}{P_2} = \frac{\overline{\Delta\lambda_{max_1}}}{\overline{\Delta\lambda_{max_2}}}, \tag{10}$$

where P_1 and P_2 are measures of the effect of deformation of single vesicles on the LSPR signal for titanium oxide and silicon oxide substrates, respectively, and $\overline{\Delta\lambda_{max_1}}$ and $\overline{\Delta\lambda_{max_1}}$ are normalized shifts of the resonance wavelength to bulk sensitivities for titanium oxide and silicon oxide substrates, respectively. We assume that a_1 and a_2 are the contact radii of a single vesicle on titanium oxide or silicon oxide, respectively. Here, the ratio P_1 [Eq. (9)] is computed as a function of a_1/r following the same convention as above. While the exact degree of deformation

of single vesicles at low coverage on titanium oxide is not known, we can see the trend in P_1 with increasing a_1/r. We also know that the normalized rate of change in the LSPR signal during the initial stage of vesicle adsorption is 1.61-times higher on silicon oxide versus titanium oxide (see Fig. 3). Taking this factor into account, namely $P_2 = 1.61P_1$, we can compute a_2 as a function of a_1 by application of Eqs. (9) and (10). This combination of theoretical model and experimental measurements allows us to quantitatively compare the extent of vesicle deformation on titanium oxide and silicon oxide.

Supporting Data

Figure S1. Comparison of experimental and simulated extinction spectra for coated gold nanodisk arrays. Experimental and 3D FDTD simulated spectra of nanodisk arrays are presented using solid and dash-dot lines, respectively. The nanodisk surface densities were selected as 7.5 and 8.6 particles/μm^2 for the silicon oxide and titanium oxide cases, respectively.

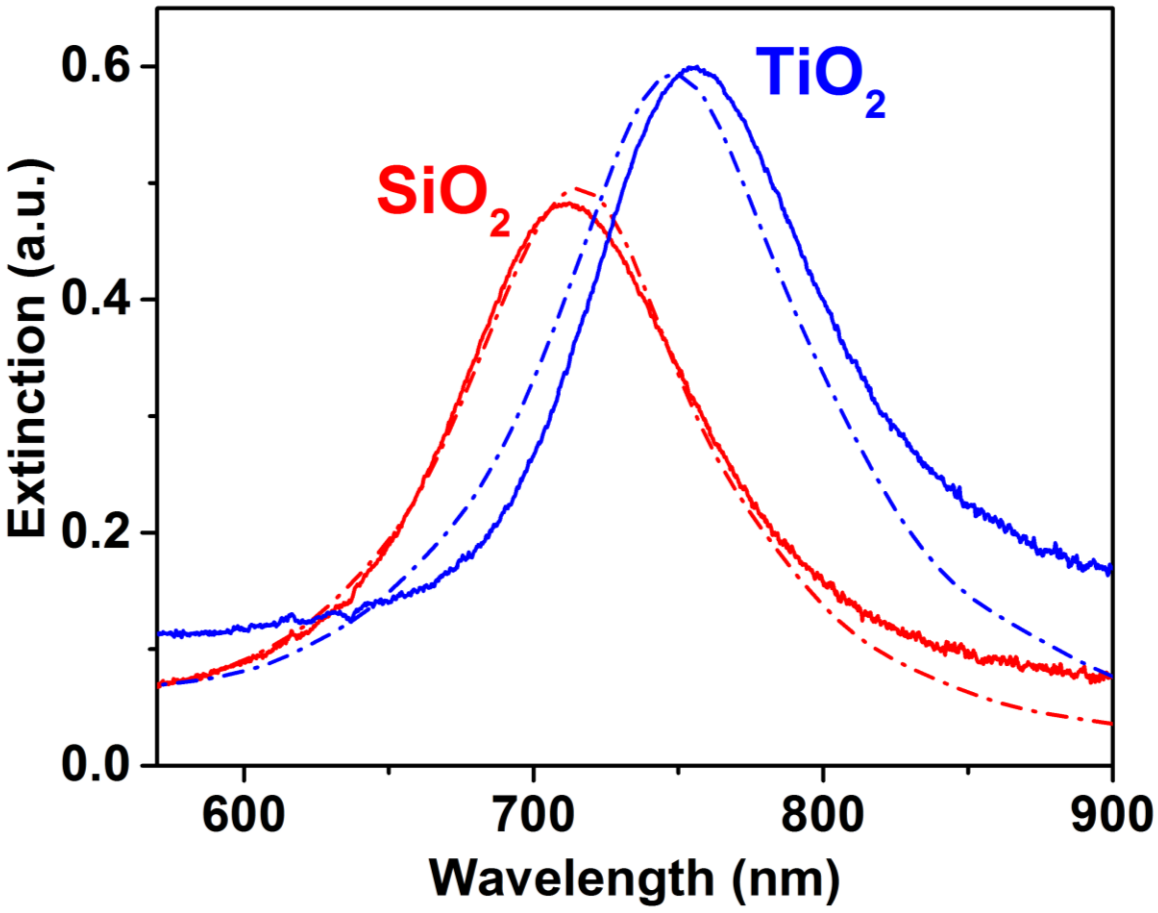

Figure S2. Derivative of the time-resolved shift in LSPR peak position (nm/min) for lipid vesicle adsorption onto the silicon oxide-coated plasmonic gold nanodisk array. Vesicle addition began around t = 5 min. **(a)** 0.4 mg/mL, **(b)** 0.2 mg/mL, **(c)** 0.1 mg/mL, **(d)** 0.05 mg/mL, **(e)** 0.025 mg/mL, and **(f)** 0.0125 mg/mL. The kinetic data is obtained from Figure 2d. Note that, at 0.4 mg/mL lipid concentration, discrete steps in the SLB formation process could not be resolved due to the relatively quick process compared to the time scale of complete solution exchange in the measurement chamber. Hence, measurement data obtained at 0.4 mg/mL lipid concentration was excluded from quantitative analysis of vesicle deformation.

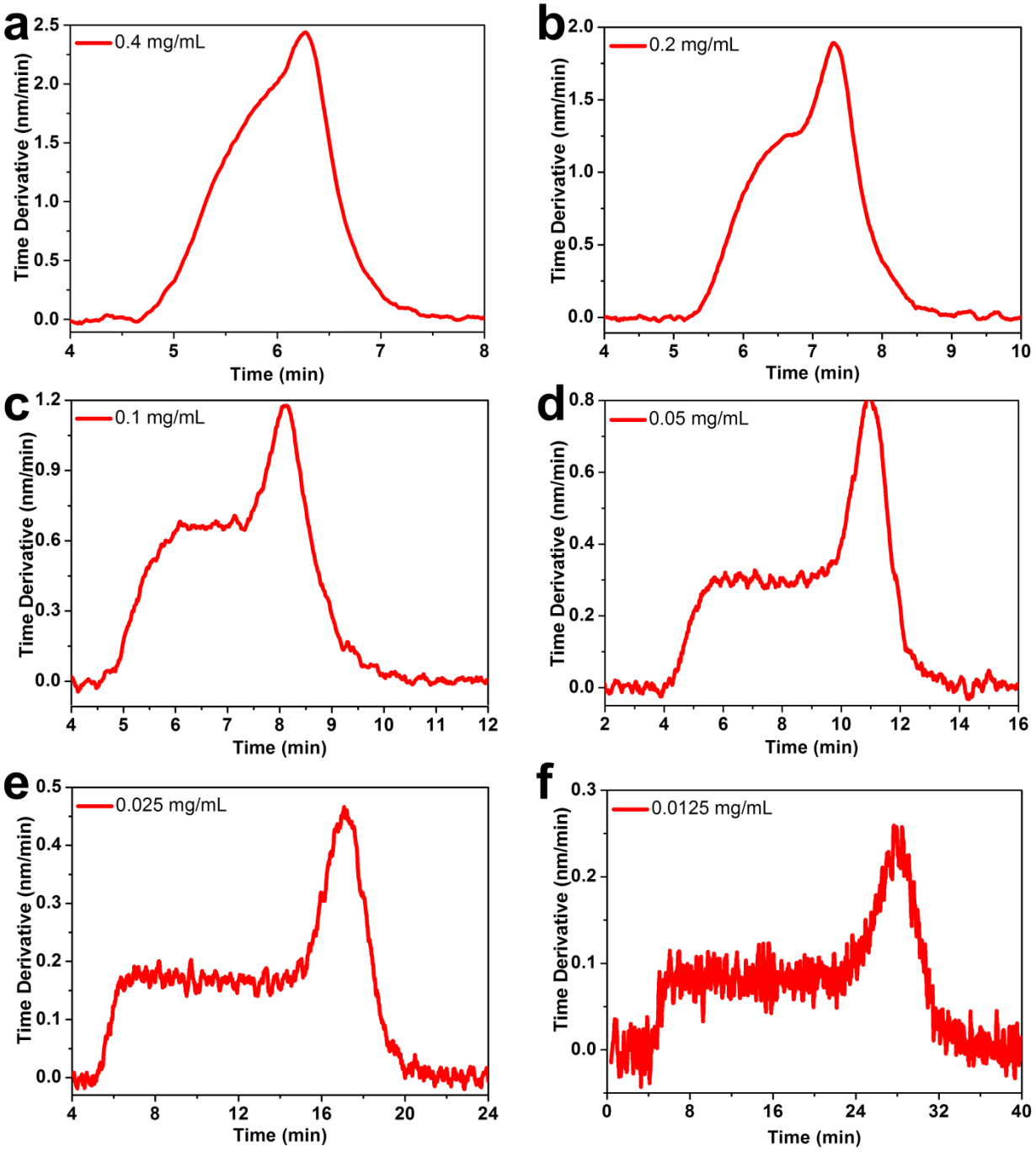

Figure S3. FRAP measurement on SLB on silicon oxide-coated gold nanodisks. Laser photobleaching was done at t = 0 s. The micrograph size is 136 x 136 μm. The intensity profile of the photobleached region is presented as a function of time during recovery of the fluorescence signal. After a laser-pulse was applied to bleach an ~20 μm wide circular spot in the bilayer, fluorescence recovery was observed and the mobile fraction was 88.2 ± 0.8 %, as compared to 90.3 ± 2.4% for an SLB on a glass coverslip reference sample. The diffusion coefficient of lateral lipid mobility was calculated to be 1.73 ± 0.04 $\mu m^2/s$ according to the Hankel transform method,[5] which is about 15% lower relative to the reference glass sample (2.04 ± 0.02 $\mu m^2/s$). The diffusivity and mobile fraction values are consistent with SLB formation, and the slightly reduced diffusion coefficient of SLBs on the nanodisk array is attributed to an increase in the effective surface area and related factors.[6]

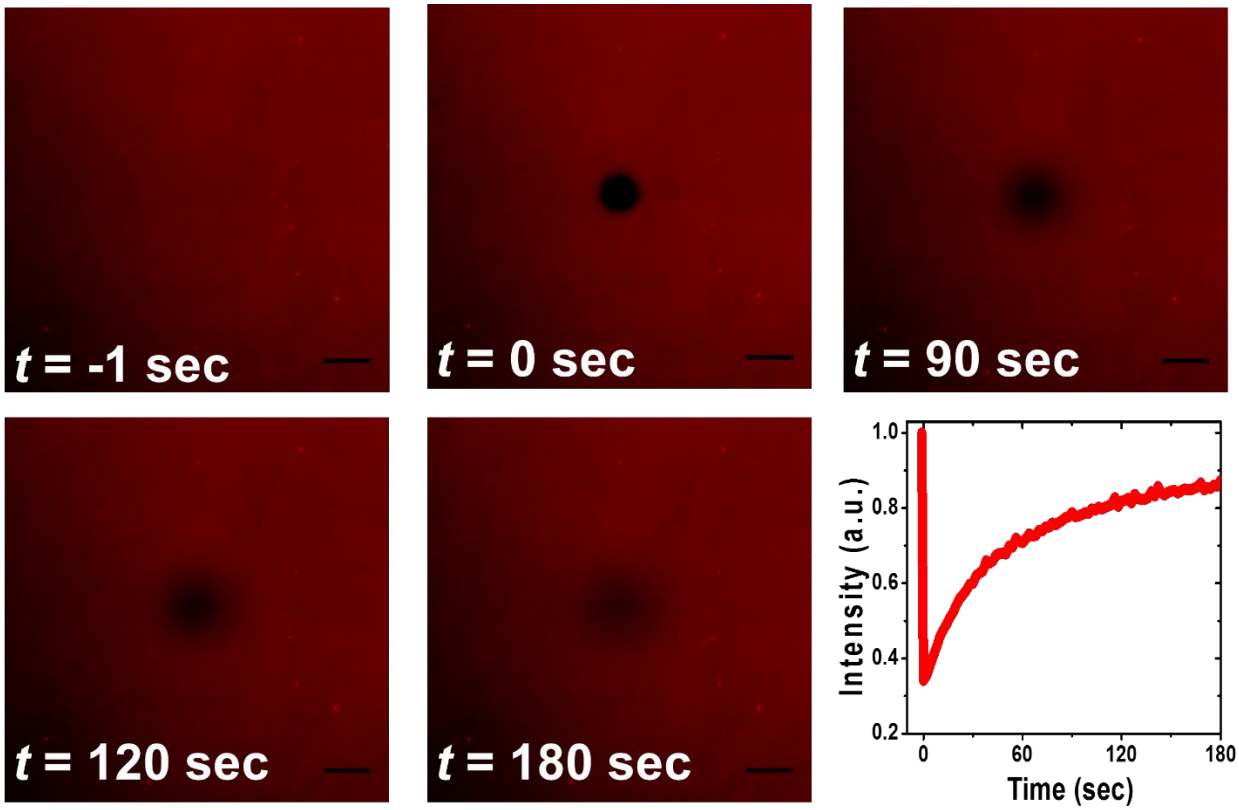

Figure S4. Comparison of time-resolved shift in LSPR peak position (nm) for lipid vesicle adsorption onto silicon oxide- and titanium oxide-coated plasmonic gold nanodisk arrays. Vesicle addition began around t = 5 min. **(a)** 0.4 mg/mL, **(b)** 0.2 mg/mL, **(c)** 0.1 mg/mL, **(d)** 0.05 mg/mL, **(e)** 0.025 mg/mL, and **(f)** 0.0125 mg/mL.

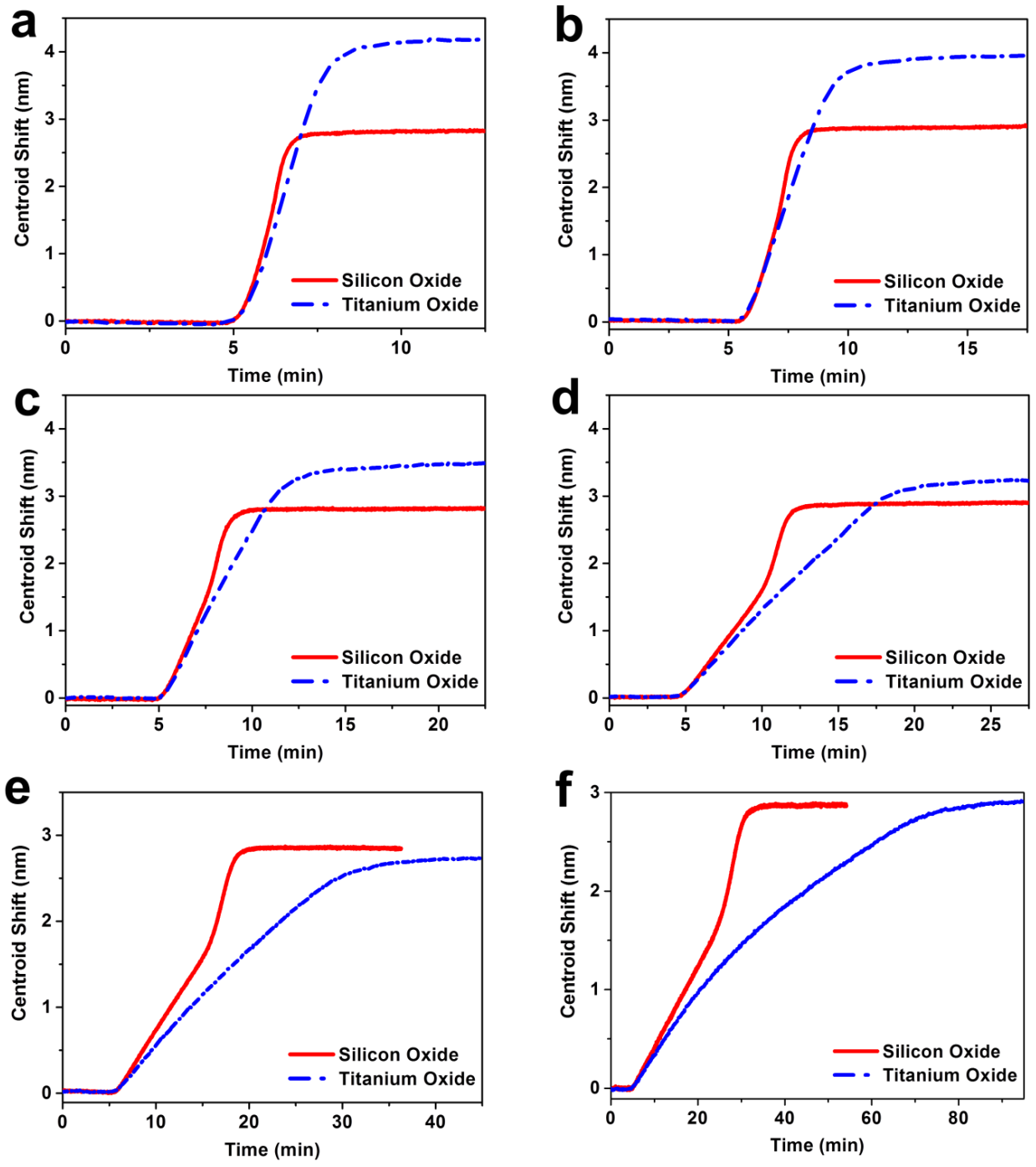

Figure S5. Comparison of time-resolved shift in LSPR peak position (RIU) for lipid vesicle adsorption onto silicon oxide- and titanium oxide-coated plasmonic gold nanodisk arrays. Vesicle addition began around t = 5 min. **(a)** 0.4 mg/mL, **(b)** 0.2 mg/mL, **(c)** 0.1 mg/mL, **(d)** 0.05 mg/mL, **(e)** 0.025 mg/mL, and **(f)** 0.0125 mg/mL.

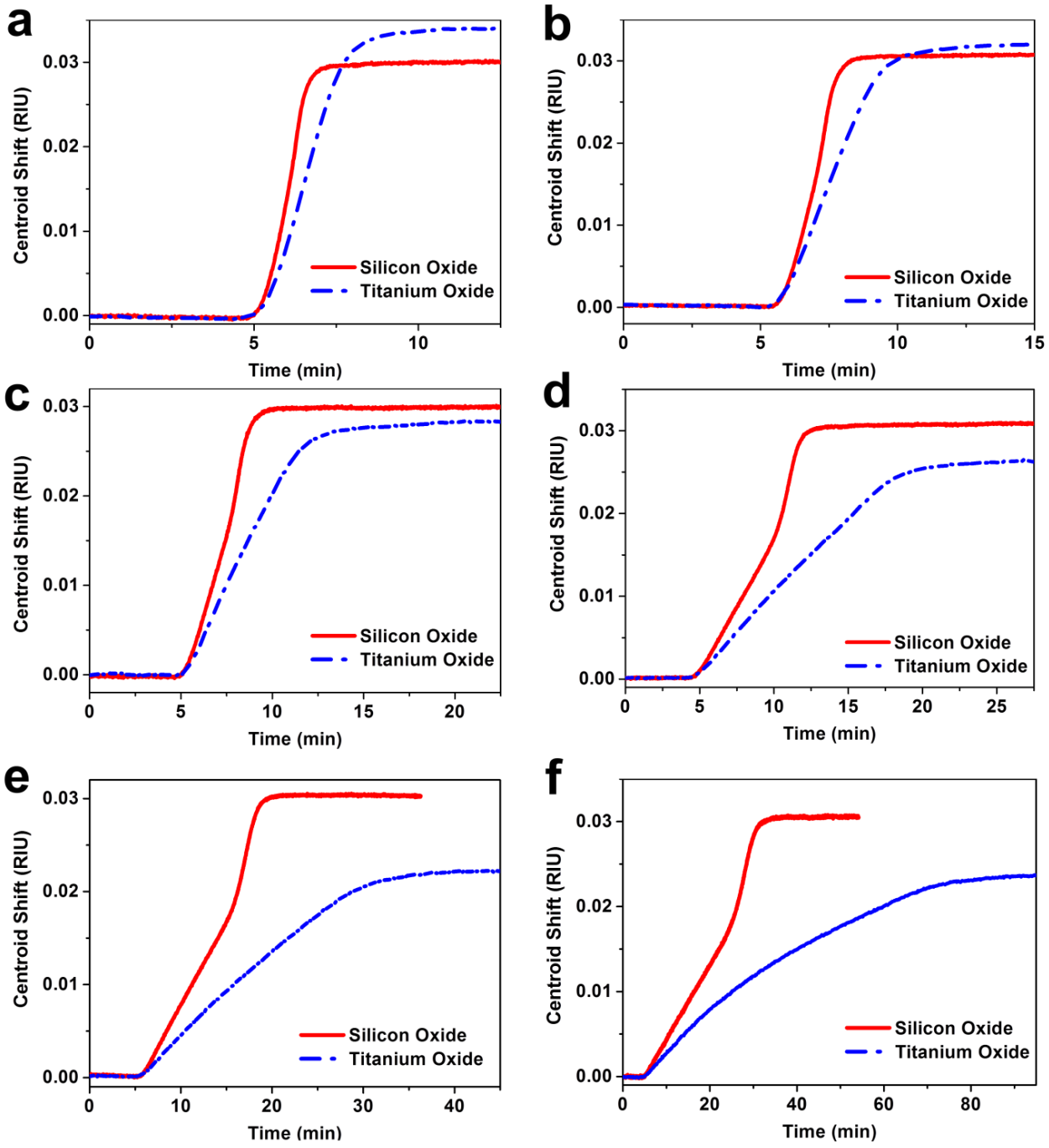

Figure S6. Comparison of derivatives of the time-resolved shift in LSPR peak position (RIU/min) for lipid vesicle adsorption onto silicon oxide- and titanium oxide-coated plasmonic gold nanodisk arrays. Vesicle addition began around t = 5 min. **(a)** 0.4 mg/mL, **(b)** 0.2 mg/mL, **(c)** 0.1 mg/mL, **(d)** 0.05 mg/mL, **(e)** 0.025 mg/mL, and **(f)** 0.0125 mg/mL.

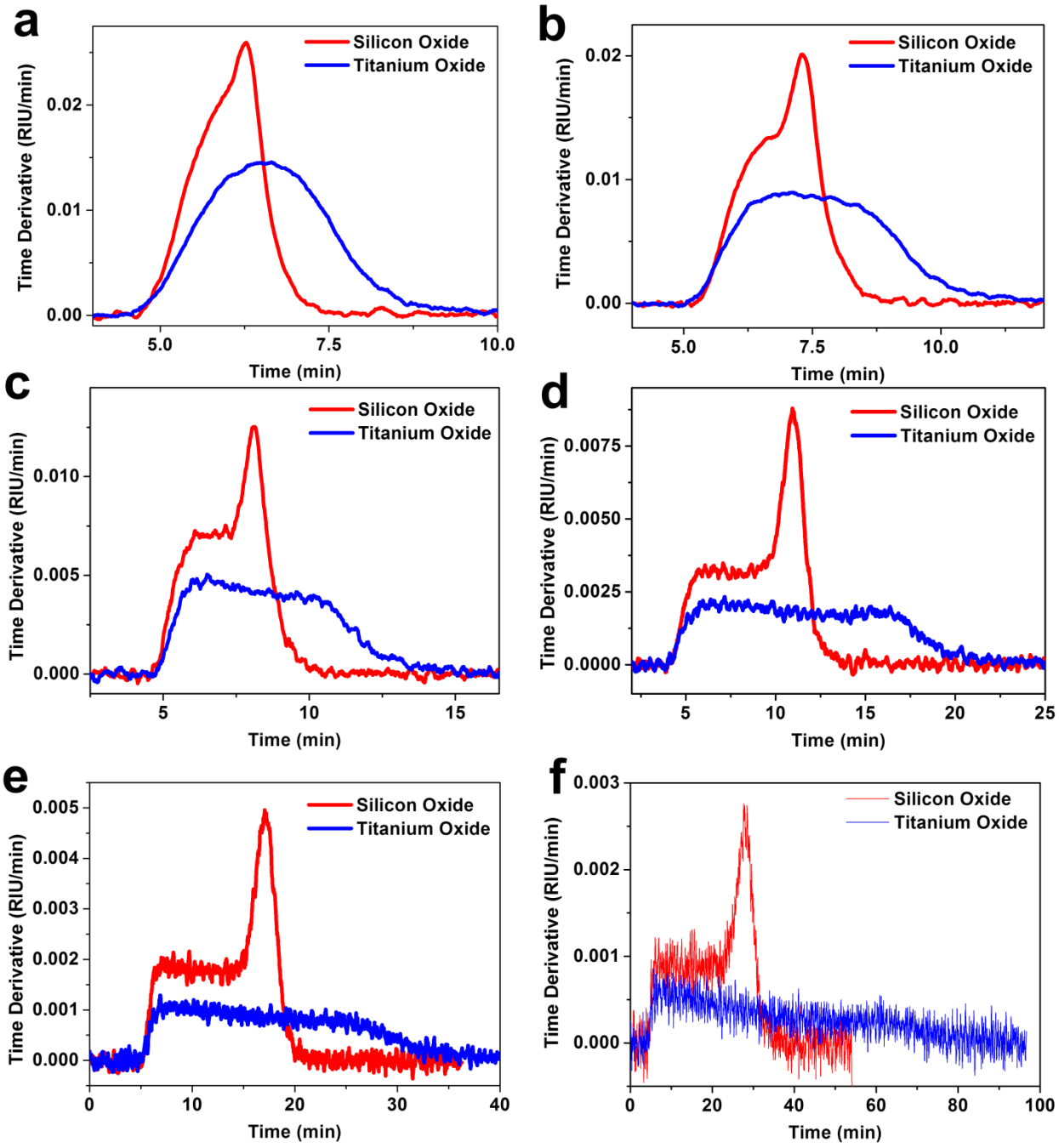

Supporting References

1. H. Z. Goh, J. A. Jackman, S.-O. Kim and N.-J. Cho, *Small*, 2014, **10**, 4828-4832.
2. P. B. Johnson and R. W. Christy, *Physical Review B*, 1972, **6**, 4370-4379.
3. J. A. Jackman, V. P. Zhdanov and N.-J. Cho, *Langmuir*, 2014, **30**, 9494-9503.
4. E. Oh, J. A. Jackman, S. Yorulmaz, V. P. Zhdanov, H. Lee and N.-J. Cho, *Langmuir*, 2015, **31**, 771-781.
5. P. Jönsson, M. P. Jonsson, J. O. Tegenfeldt and F. Höök, *Biophysical Journal*, 2008, **95**, 5334-5348.
6. M. P. Jonsson, P. Jönsson, A. B. Dahlin and F. Höök, *Nano Letters*, 2007, **7**, 3462-3468.